ANALOG FILTERS

ACTIVE-RC FILTERS

INDUCTORLESS FILTERS

ANALOG ACTIVE-RC FILTERS

ACTIVE FILTERS

FILTERS, ANALOG

An electrical filter is a device, circuit, or system that transforms a given input signal into a desired output signal. The transformation or filtering may be carried out in the frequency or the time domain, and by a variety of physical means (electrical, mechanical, acoustical, etc.) depending on the frequency range of the signals, on the available technology, and on the application in question. The most commonly used electrical filters have traditionally been wave or frequency filters, although with the development of highly sophisticated digital signal processors on a silicon integrated chip, filtering in the time domain has become equally feasible. Because this article deals with analog filtering, we restrict ourselves to filtering issues in the frequency domain.

FILTER CATEGORIES

Electrical filters can be categorized in a number of ways: for example, functionally (high-pass, low-pass, bandpass, etc.), technologically by component type or physical medium [inductor–capacitor–resistor (*LCR*), mechanical, active *RC,* active g_m–*C*, monolithic crystal, quartz, etc.], or by their operational features. Referring to Fig. 1, we consider the last categorization here. The figure shows the three main modes in which a filter can operate. Altogether from input to output, we have an analog filter, that is, a filter that is continuous in amplitude and time. If we sample the incoming signal in time [after bandlimiting the signal with an antialiasing filter (*AAF*)] but leave the amplitude continuous (nonquantized), we have a so-called sampled-data, or discrete-time, filter. If now we also quantize the amplitude by passing the signal through an analog-to-digital converter (*ADC*), we have a digital filter. In either case, sampled-data or digital, if we require an analog signal at the output, we must add a digital-to-analog converter (*DAC*) and a reconstruction filter to the processing chain. Although filters operating in continuous time and amplitude, as well as those operating in discrete time but nonquantized amplitude (i.e., sampled-data filters) are sometimes referred to as analog filters, in this article we shall include only the former in this category. Sampled-data filters, and in particular switched-capacitor filters, are dealt with separately under ***Switched capacitor circuits***. For other categorizations of filters, see also ***Classical filter synthesis***.

TRANSFER FUNCTION AND FREQUENCY RESPONSE

Classical filters are made up of inductors (L), capacitors (C), and terminating resistors (R); thus they are often referred to as *LCR* filters. Ideally, the inductors and capacitors are considered to be lossless, the only lossy components being the terminating resistors. The synthesis of such filters is dealt with under ***Classical Filter Synthesis***. Interestingly enough, most analog (and much digital) filtering can be traced back to, and derived from, the foundations of classical *LCR*-based filter theory.

LCR filters belong to the family of linear, lumped-parameter, finite (*LLF*) networks. Those not falling into this category typically are nonlinear, distributed (e.g., individual components such as resistors and capacitors cannot be identified, but are distributed filmlike on a substrate), nonfinite, or any combination of these. The *order* of an LLF filter is related to the number of reactive, or lossless, components in the network. For example, if a low-pass filter comprises one inductor, one capacitor, and two resistors, it is of second order.

The output signal of an nth-order LLF network can generally be found in terms of the input signal by solving a linear nth-order differential equation of the form

$$a_n\frac{d^n y}{dt^n}+a_{n-1}\frac{d^{n-1}y}{dt^{n-1}}+\cdots+a_1\frac{dy}{dt}+a_0 y = b_m\frac{d^m x}{dt^m}+b_{m-1}\frac{d^{m-1}x}{dt^{m-1}}+\cdots+b_1\frac{dx}{dt}+b_0 x \quad (1)$$

where $x(t)$ is the input signal, $y(t)$ is the output signal, and $n \geq m$. Applying the Laplace transform to this equation, we obtain the transfer function $T(s) = Y(s)/X(s)$ as the ratio of two polynomials $N(s)$ and $D(s)$, namely,

$$T(s)=\frac{N(s)}{D(s)}=\frac{b_m s^m+b_{m-1}s^{m-1}+\cdots+b_1 s+b_0}{a_n s^n+a_{n-1}s^{n-1}+\cdots+a_1 s+a_0} \quad (2)$$

where $s=\sigma+j\omega$ is the complex frequency and $N(s)$ and $D(s)$ are polynomials in s with real coefficients a_i and b_j. Expressing $N(s)$ and $D(s)$ in their factored form, we obtain the poles and zeros of the transfer function:

$$T(s)=K\frac{(s-z_1)(s-z_2)\cdots(s-z_m)}{(s-p_1)(s-p_2)\cdots(s-p_n)}=K\frac{\prod_{i=1}^{m}(s-z_i)}{\prod_{j=1}^{n}(s-p_j)} \quad (3)$$

As the coefficients a_i and b_j in Eq. (2) are real, the poles p_j and zeros z_i must be either real or complex conjugate. The factor K is a scaling factor whose dimension is such as to render the transfer function $T(s)$, when it is a voltage or a current ratio, dimensionless. Combining a complex conjugate zero pair with a complex conjugate pole pair, we obtain the special case of a second-order transfer function:

$$T(s)=K\frac{(s-z)(s-z^*)}{(s-p)(s-p^*)}=K\frac{s^2+(\omega_z/q_z)s+\omega_z^2}{s^2+(\omega_p/q_p)s+w_p^2} \quad (4)$$

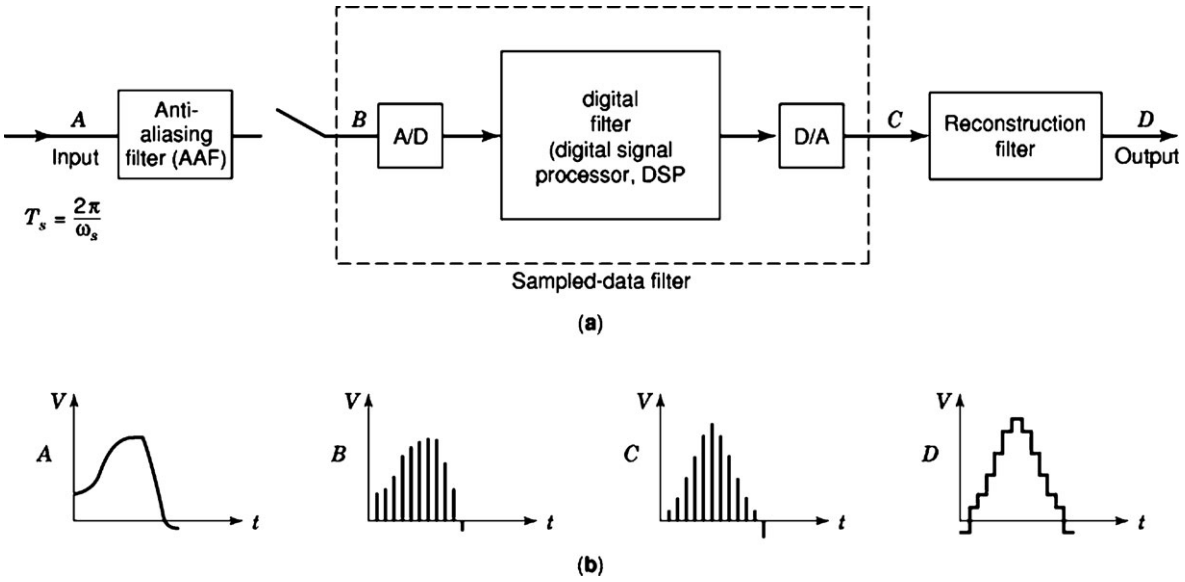

Figure 1. Diagram of a generalized filter, demonstrating analog, sampled-data, and digital signal processing: (a) block diagram including input sampler and output reconstruction filter; (b) typical waveforms at points A through D.

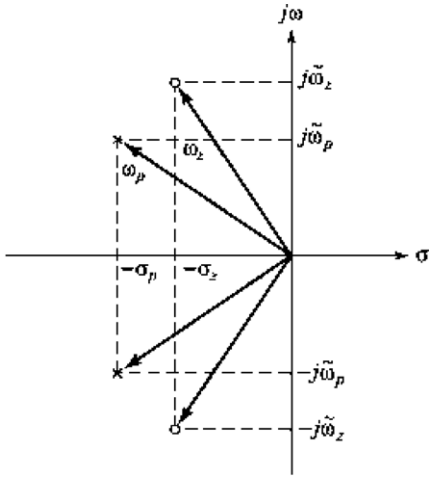

Figure 2. The pole–zero diagram of a general second-order transfer function.

where

$$z, z^* = -\sigma_z \pm j\tilde{\omega}_z$$
$$p, p^* = -\sigma_p \pm j\tilde{\omega}_p \qquad (5)$$

The poles and zeros can be displayed in the complex frequency, or s, plane as shown in Fig. 2. Note that

$$\omega_z^2 = \sigma_z^2 + \tilde{\omega}_z^2, \qquad \omega_p^2 = \sigma_p^2 + \tilde{\omega}_p^2 \qquad (6)$$

and

$$q_z = \frac{\omega_z}{2\sigma_z}, \qquad q_p = \frac{\omega_p}{2\sigma_p} \qquad (7)$$

To obtain the frequency response of a filter described by Eq. (1), we assume a sinusoidal input signal and, because the network is linear, obtain a sinusoidal response. The response is obtained by letting $s = j\omega$ in Eq. (3); thus,

$$T(j\omega) = K\frac{\prod_{i=1}^{m}(j\omega - z_i)}{\prod_{j=1}^{n}(j\omega - p_j)} = |T(j\omega)|e^{j\phi(\omega)} \qquad (8)$$

Taking the natural logarithm of $T(j\omega)$, we obtain

$$\ln T(j\omega) = \ln|T(j\omega)| + j\arg T(j\omega) = \alpha(\omega) + j\phi(\omega) \qquad (9)$$

where $\alpha(\omega)$ and $\phi(\omega)$ are the gain and phase response, given in nepers and degrees, respectively. To obtain the gain response in decibels, we have

$$\alpha_{\mathrm{dB}}(\omega) = 20\log|T(j\omega)| = \frac{20}{\ln 10}\alpha(\omega) = 8.686\alpha(\omega) \qquad (10)$$

and to obtain the group delay,

$$\tau_g(\omega) = -\frac{d\phi(\omega)}{d\omega} \qquad (11)$$

Typically frequency-selective filters are classified according to their frequency or phase response, and each response has its characteristic pole–zero pattern in the complex frequency, (s) plane. For reasons of stability, all poles must be in the left half plane (*LHP*) excluding the $j\omega$ axis. Thus, for example, the maximally flat or Butterworth low-pass filter will have poles distributed on a semicircle centered at the origin in the left half s plane, and the equiripple or Chebyshev low-pass filter will have its LHP poles on an ellipse with center at the origin. In fact, it can generally be stated that the poles of any practical frequency-selective filter must have complex conjugate LHP poles. The only other practical alternative is for the poles to lie on the negative real axis, which is the domain of inductorless, passive *RC* networks. It can readily be shown that such filters, although perfectly stable and easily designable, are rarely of any practical use because their in-band frequency se-

lectivity is extremely poor. Thus, for example, where the center-frequency-to-3 dB-bandwidth ratio of a practical *LCR* second-order bandpass filter can be arbitrarily high (limited only by the nonideal characteristics of the inductors and capacitors), that same ratio of its passive *RC* counterpart will be less than 0.5. [An easy way to show this is as follows: Referring to Eq. (1), assume that the two negative-real poles of a passive *RC* bandpass filter are at $-\sigma_1$ and $-\sigma_2$ on the negative-real axis in the complex-frequency s-plane. Then we have $(s+\sigma_1)(s+\sigma_2) = s^2 + (\sigma_1+\sigma_2)s + \sigma_1\sigma_2$ with σ_1, σ_2 real and strictly positive. By identification with $s^2 + (\omega_p/q_p)s + \omega^2{}_p$ we then have $\omega_p = \sqrt{\sigma_1\sigma_2}$ and $\omega_p/q_p = \sigma_1 + \sigma_2$, or $1/q_p = \sqrt{\sigma_1/\sigma_2} + \sqrt{\sigma_2/\sigma_1}$. Letting $x = \sqrt{\sigma_1/\sigma_2}$ we therefore have $1/q_p = x + 1/x$, which is a parabolic-like function whose minimum is equal to 2 for $x = 1$, or $\sigma_1 = \sigma_2$. Thus, $(1/q_p)_{\min} = 2$, i.e., $(q_p)_{\max} = 0.5$. However, because a passive *RC* network may have no multiple poles (e.g., a double pole results in an infinite spread of the *RC* component values), it follows that σ_1 may not be equal to σ_2, i.e., $\sigma_1 \neq \sigma_2$, and the *RC* pole q_p, which we have designated $\hat{Q}_p$, must be less than 0.5. Finally, because for a second-order band-pass filter, q_p is identically equal to the ratio of the center frequency to the 3 dB bandwidth, it follows that for an *RC* band-pass filter this ratio must be *less* than 0.5]. It is this characteristic feature of passive *RC* networks—namely that their poles must lie on the negative real axis in the s plane, thereby drastically reducing their capability of frequency selection—that leads to the basic problem of so-called inductorless filters.

The Problem of Inductorless Filters

We have indicated above that the transfer-function poles of any practical frequency-selective filter (Butterworth, Chebyshev, inverse Chebyshev, elliptic or Cauer, Bessel, etc.) must be complex conjugate. In terms of the quantity q_p [the so-called pole Q, which is given by Eq. (7)], this means that for any complex conjugate pole pair $p_i, p^*{}_i$, the corresponding q_{pi} must be greater than 0.5. Note that with the *LCR* filters of classical filter theory, we have no trouble realizing such complex conjugate pole pairs. However, inductors are incompatible with integrated circuit technology, and with small-size hand-held equipment, at least at frequencies below several megahertz. This is because the needed inductance and hence the physical size of inductors increases with decreasing operational frequencies. Consequently, the trend is to eliminate inductors from electronic equipment wherever possible, leaving, in the case of *LCR* filters, only *RC* circuits behind. As we have seen, however, because the poles of *RC* circuits and filters are restricted to the negative real axis, such inductorless *RC* filters, per se, are useless for most practical filter design. In fact, denoting the pole Q of a second-order passive *RC* network by $\hat{Q}_p$, it was shown above that $\hat{Q}_p < 0.5$. As we shall see in what follows, with the inclusion of gain cells or amplifiers, this critical limitation can be readily overcome.

CASCADED ACTIVE *RC* BIQUADS

Cascaded biquad filter design is one of the oldest, and has proved to be one of the most useful, of active *RC* filter design methods. This is mainly due (1) to their simplicity of design—viz., second-order (or third-order) filter sections, or *biquads,* can be cascaded to provide any nth-order filter function—and (2) to the excellent properties and low cost of silicon integrated (CMOS and bipolar) voltage and current amplifiers.

Foremost among the voltage amplifiers, the operational amplifier, or *opamp,* is ideally a differential-input, single-ended, or differential-output amplifier with infinite gain, infinite bandwidth and input impedance, and zero output impedance and offset voltage. In practice the gain may be anywhere between 60 dB and 100 dB, the bandwidth several tens to hundreds of megahertz, and the input impedance several tens to hundreds of megohms. The offset voltage may be several to tens of millivolts. These features may be mutually exclusive; an opamp will be designed to optimize one or more of them, and in addition numerous others, such as dissipated power, noise, common-mode and power-supply-rejection ratio, slew rate, and so on. As a network element, the idealized opamp can be considered to be a voltage-controlled voltage source with infinite gain and, when used with negative feedback, a virtual ground at the input.

More recently, current amplifiers are also being used in the form of operational transconductance amplifiers (*OTAs*), current feedback amplifiers, and current conveyors. To a large extent these current-based amplifiers are duals of the voltage-based opamps. They have certain technology-related advantages when built into CMOS or BiCMOS technology, and are often advantageous with respect to required power and high-frequency operation. In what follows the conventional opamp is assumed as the basic gain element; the change to current-based amplifiers generally has very little consequence with respect to the theoretical, and even to the practical, design aspects.

Recall from the above that the transfer function of an nth-order filter network has the form given by Eq. (2), where $T(s)$ is a rational function in the complex frequency variable s. The order of $T(s)$ is determined by the order of the denominator polynomial $D(s)$. $T(s)$ can be factored into a product of second- or third-order functions $T_i(s)$, according to n being even or odd. Thus, for n even,

$$T(s) = \prod_{i=1}^{n/2} T_i(s) \tag{12}$$

and for n odd,

$$T(s) = \frac{1}{s+\alpha} \prod_{i=1}^{(n-1)/2} T_i(s) \tag{13}$$

where α is a negative real pole and the individual biquadratic functions $T_i(s)$ have the general form

$$T_i(s) = K_i \frac{s^2 + \frac{\omega_{z_i}}{q_{z_i}} s + \omega_{z_i}^2}{s^2 + \frac{\omega_{p_i}}{q_{p_i}} s + \omega_{p_i}^2} = K_i \frac{(s-z_i)(s-z_i^*)}{(s-p_i)(s-p_i^*)} \tag{14}$$

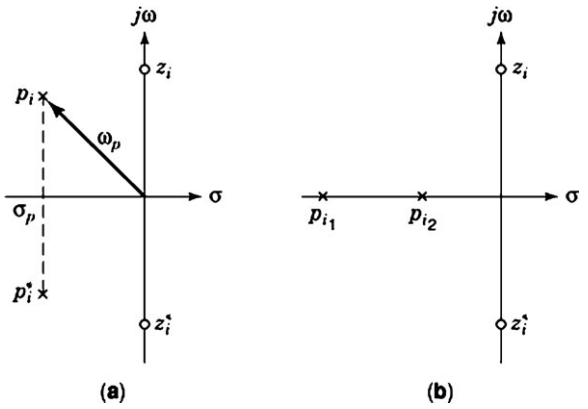

Figure 3. Typical pole–zero pair: (a) of an elliptic *LCR* biquad filter, $q_p = \omega_p/2\sigma_p$; (b) passive *RC* biquad filter, $p_{i1}\ p_{i2} = \omega^2{}_p$, $\hat{Q}_p = \omega_p/(p_{i1} + p_{i2})$, $\hat{\sigma}_p = (p_{i1} + p_{i2})/2$.

For most practical applications the poles of each biquad function $T_i(s)$ will be complex conjugate, as shown in Fig. 3(a). The location of the zeros is less significant with regard to their realization. Complex conjugate zeros are realizable both with *LCR* and with passive *RC* networks. [Zeros on the imaginary axis (as shown in Fig. 3) correspond to so-called elliptic or inverse Chebyshev filters.] The closer the poles are to the $j\omega$ axis, the higher will be the selectivity of the filter; the closer the zeros, the larger the filter attenuation at those frequencies. Referring to Eqs. 6 and 7, the proximity to the $j\omega$ axis of the poles and zeros is indicated by the quantities q_p and q_z, respectively; the closer they are to the $j\omega$ axis, the higher the q values will be. If, on the other hand, the critical frequencies (i.e., poles and zeros) are on the negative real axis, that is, far from the $j\omega$ axis, the corresponding q values will be less than 0.5; if they are complex conjugate, the q values will be larger than 0.5 and, in the limit (i.e., on the $j\omega$ axis), equal to infinity. For the pole Q (i.e., q_p) this latter case is forbidden, because poles on, or to the right of, the $j\omega$ axis correspond to an unstable network.

As pointed out above, it can be shown that the poles of a passive *RC* network must be single and on the negative real axis [see Fig. 3(b)], whereas there is no such limitation on the location of the zeros. In terms of q_p this means that for a second-order *RC* network, that is, for a pole pair on the negative real axis,

$$(q_p)_{RC} = \hat{q}_p < 0.5 \tag{15}$$

where we use the circumflex on q, and on any other pertinent quantity describing the network, to indicate that it is associated with a *passive RC* network. On the other hand, we have seen that for any practical application, the selectivity specifications of the filter will require complex conjugate poles:

$$(q_p)_{LCR} = q_p > 0.5 \tag{16}$$

As indicated in this expression, this condition is readily satisfied by conventional *LCR* networks. Thus, the basic difference between a passive *RC* and a passive *LCR* network is the location of the poles: a passive *RC* network has negative real poles and consequently poor frequency selectivity; an *LCR* network can, theoretically have poles arbitrarily close to, but not on, the $j\omega$ axis, and therefore its frequency selectivity is, theoretically, almost unlimited. Thus, in an *active RC* network, the purpose of a gain element (whose gain we denote by β) is essentially to increase the $\hat{Q}_p$ of each pole pair to a value q_p that is larger than 0.5. This can be done in a number of different ways.

Single-Amplifier Biquads (Sallen–Key Biquads)

The *biquad* (biquadratic filter cell) is a building block whose transfer function is given by Eq. (14), with the possible inclusion of a negative real pole α as in Eq. (13). The negative real pole can be realized by a simple passive *RC* low-pass combination attached to the active biquad. Strictly speaking, the biquad is then of third order, but the active feedback part of the filter remains second-order and provides the complex conjugate pole pair.

Since power is generally at a premium in electronic equipment, it is desirable, wherever possible, to realize the biquad with as few amplifiers or gain devices as possible. For low-to-medium pole Q's, single-amplifier biquads are therefore not only feasible and, in most cases, adequate, but also very desirable.

There are two basic categories of single-amplifier biquads: those based on negative, and those based on positive feedback. The former can be grouped into three distinct classes, the latter into one. Because one of the earliest publications on active biquads using single (vacuum-tube) amplifiers was by R. P. Sallen and E. L. Key (1), single-amplifier biquads are often referred to as "Sallen–Key biquads" (even though modern single-amplifier biquads have little in common with those early units). The basic principles underlying these biquads are outlined in what follows.

Negative-Feedback Biquads (Q Multiplication). We start out with the biquadratic transfer function $\hat{T}(s)$ of a passive (no gain element) *RC* second-order network,

$$\hat{T}(s) = \frac{N(s)}{s^2 + (\omega_p/\hat{q}_p)s + \omega_p^2} \tag{17}$$

The poles of this function are, by definition, negative real, i.e., $\hat{Q}_p < 0.5$. Multiplying $\hat{Q}_p$ by a quantity μ such that

$$\mu = 1 + \beta \quad \text{and} \quad \beta > 0 \tag{18}$$

we obtain the same function as in Eq. (17), except that it now has complex conjugate poles:

$$T(s) = \frac{N(s)}{s^2 + (\omega_p/q_p)s + \omega_p^2} \tag{19}$$

where

$$q_p = \hat{q}_p(1 + \beta) > 0.5 \tag{20}$$

Note that β must be selected to satisfy Eq. (20). It therefore depends on the value of $\hat{Q}_p$, and on the required value q_p. After some manipulation, and with the assumption that

$\beta > 1$, Eq. (19) can be written as

$$T(s) = \hat{T}(s)\frac{\beta}{1+\beta\hat{t}_1(s)} \tag{21}$$

where

$$\hat{t}_1(s) = \frac{s^2+\omega_p^2}{s^2+(\omega_p/\hat{q}_p)s+\omega_p^2} \tag{22}$$

Equation (21) corresponds to the transfer function of an active RC biquad consisting of $\hat{T}(s)$, $\hat{t}_1(s)$, and the amplifier β, connected in a negative-feedback loop as shown in the block diagram of Fig. 4. A typical biquad with band-pass characteristics, which is based on Q multiplication, is shown in Fig. 5.

Positive-Feedback Biquads (Sigma Reduction). Instead of expressing the transfer function of the initial second-order RC network in terms of $\hat{Q}_p$ as in Eq. (17), we can do so in terms of the negative real quantity $\hat{\sigma}_p$, thus:

$$\hat{T}(s) = \frac{N(s)}{s^2+2\hat{\sigma}_p s+\omega_p^2} \tag{23}$$

where

$$\hat{\sigma}_p > \omega_p \tag{24}$$

The inequality Eq. (24) indicates that the two poles of $\hat{t}(s)$ are negative real. They can be made complex conjugate by decreasing the quantity $2\hat{\sigma}_p$ by some amount κ:

$$T(s) = \frac{N(s)}{s^2+(2\hat{\sigma}_p-\kappa)s+\omega_p^2} \tag{25}$$

where

$$0 < \kappa < 2\hat{\sigma}_p \tag{26}$$

Equation (25) now corresponds to Eq. (19), since

$$q_p = \frac{\omega_p}{2\hat{\sigma}_p-\kappa} > 0.5 \tag{27}$$

meaning that $T(s)$ in Eq. (25) now has complex conjugate poles. $T(s)$ can now be rewritten as

$$T(s) = \frac{1}{\kappa}\hat{T}(s)\frac{\kappa}{1-\kappa\hat{t}_2(s)} \tag{28}$$

where

$$\hat{t}_2(s) = \frac{s}{s^2+2\hat{\sigma}_p s+\omega_p^2} \tag{29}$$

Equation (28) corresponds to an RC network consisting of $\hat{T}(s)$ and $\hat{t}_2(s)$ connected in a positive-feedback configuration with gain κ. This is shown in the block diagram of Fig. 6. A low-pass biquad based on sigma reduction, that is, positive feedback, is given in Fig. 7.

A Classification of Single-Amplifier Biquads. It was shown above that complex conjugate poles can be generated by Q multiplication or sigma reduction applied to a second-order passive RC filter network. The former method is based on negative, the latter on positive feedback. Both can be represented by the general feedback structure shown in Fig. 8. Here the RC network in the forward path, $\hat{t}_{12}(s)$, determines the filter type (low-pass, high-pass, band-pass, etc.). The RC network in the feedback path, $\hat{t}_{32}(s)$, determines the necessary feedback polarity and the actual path on the root locus with respect to β, along which the initially negative-real poles of $\hat{t}_{32}(s)$ move, to become the complex conjugate poles of $T(s)$. It can be shown that there are essentially three basic feedback functions $\hat{t}_{32}(s)$ providing complex conjugate poles with negative feedback, and one basic feedback function $\hat{t}_{32}(s)$ providing them with positive feedback. The individual $\hat{t}_{32}(s)$ functions are the transfer functions of second-order passive RC networks providing a low-pass, high-pass, and band-stop filter function in the first three classes, respectively, and a band-pass function in the fourth class. This is the basis for the classification of single-amplifier biquads presented in Table 1.

Which of these biquads should be used to obtain a particular filter type depends on the application. More on this and other practical design questions can be found in the publications referred to in the reading list at the end of this article.

Multiple-Amplifier Biquads (State-Variable Biquads)

The biquads in the multiple-amplifier category start out from the nth-order transfer function given by Eq. (2), just as the single-amplifier biquads did. However, rather than individually shifting the pole Q's of passive RC networks into the complex-frequency plane with the help of negative or positive feedback, this method converts the transfer function into a function of interconnected integrators, which can be graphically represented by a so-called state-variable signal-flow graph (hence the name "state-variable biquads"). The method requires at least as many amplifiers as the order of the transfer function (in the case of a biquad it actually requires three opamps) and is therefore not economical of power. This disadvantage is compensated for by a flexibility in terms of pole-frequency tuning, in that the pole frequency and Q can be adjusted, or *tuned,* independently of one another. The method is not restricted to biquads and can be directly applied to an nth-order transfer function (hence this method is often referred to as the "direct-form" active filter design). Because of stability and sensitivity problems with higher than second-order networks, the method is practically restricted to biquad design. In what follows we shall therefore illustrate the method for a general second-order filter function, or biquad.

Consider the general biquadratic function $T(s)$ [which corresponds to that given by Eq. (14)]:

$$T(s) = K\frac{s^2+B_1 s+B_0}{s^2+A_1 s+A_0} = K\frac{s^2+\dfrac{\omega_z}{q_z}s+\omega_z^2}{s^2+\dfrac{\omega_p}{q_p}s+\omega_p^2} \tag{30}$$

Note that in the general case the coefficient B_1 can be positive or negative, corresponding to finite zeros in the left or right half plane, respectively. (Networks with left- and right-half-plane zeros are often referred to as minimum-phase and non-minimum-phase networks, respectively.) By

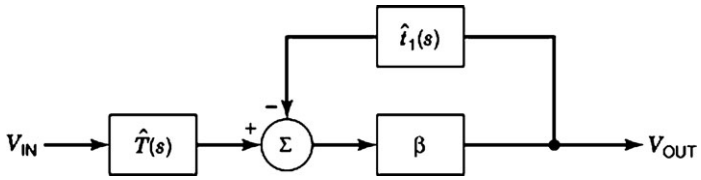

Figure 4. Block diagram, based on negative feedback, of an active *RC* biquad with complex conjugate poles.

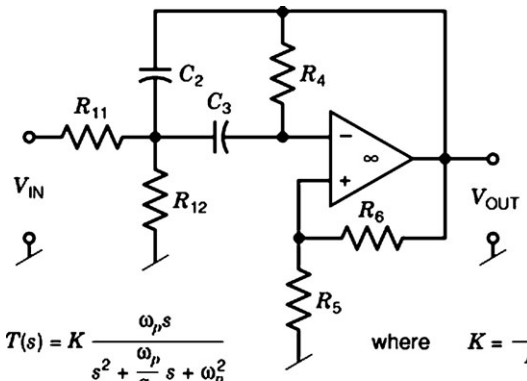

$$T(s) = K\frac{\omega_p s}{s^2 + \frac{\omega_p}{q_p}s + \omega_p^2} \quad \text{where} \quad K = \frac{R_{12}}{R_{11}+R_{12}}\left(1+\frac{R_5}{R_6}\right)\sqrt{\frac{R_4C_3}{R_1C_2}}$$

$$\omega_p^2 = \frac{1}{R_1C_2C_3R_4}$$

$$q_p = \frac{\sqrt{R_4C_2/R_1C_3}}{1 + C_2/C_3 - R_4R_5/R_1R_6}$$

$$R_1 = R_{11} \parallel R_{12}$$

Figure 5. A band-pass filter biquad based on negative feedback.

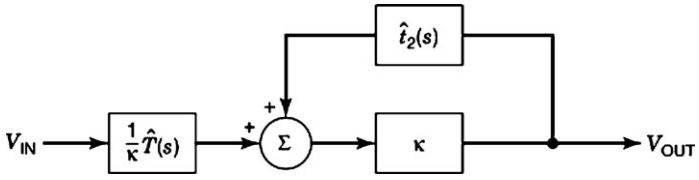

Figure 6. Block diagram, based on positive feedback, of an active *RC* biquad with complex conjugate poles.

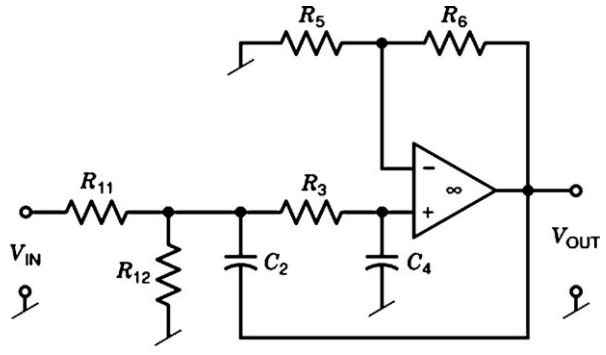

$$T(s) = K\frac{\omega_p^2}{s^2 + \frac{\omega_p}{q_p}s + \omega_p^2} \quad \text{where} \quad K = \frac{R_{12}}{R_{11}+R_{12}}\left(1+\frac{R_6}{R_5}\right)$$

$$\omega_p^2 = \frac{1}{R_1C_2R_3C_4}$$

$$q_p = \frac{\sqrt{R_3C_2/R_1C_4}}{1 + R_3/R_1 - R_6C_2/R_5C_4}$$

$$R_1 = R_{11} \parallel R_{12}$$

Figure 7. A low-pass filter biquad based on positive feedback.

Table 1. Classification of Single-Amplifier Biquads

Class	$\hat{t}_{32}(s)$	Realizable Filter Functions $T(s)$
	Negative Feedback	
1	Low-pass	Low-pass Band-pass
2	High-pass	High-pass Band-pass
3	Band-stop	Low-pass High-pass Band-pass
	Positive Feedback	
4	Band-pass	Low-pass High-pass Band-pass Band-stop

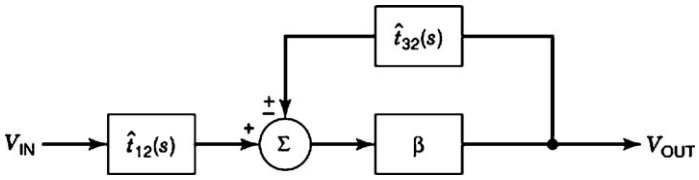

Figure 8. A general feedback configuration, which serves as the basis for single-amplifier active *RC* biquads.

contrast, A_1 *must* be positive and greater than zero, because the poles *must* lie in the left-half plane excluding the $j\omega$ axis.

Dividing the numerator and denominator of $T(s)$ by s^2, we obtain

$$T(s) = K\frac{1+B_1\left(\frac{1}{s}\right)+B_0\left(\frac{1}{s}\right)^2}{1+A_1\left(\frac{1}{s}\right)+A_0\left(\frac{1}{s}\right)^2} = K\frac{1+\frac{\omega_z}{q_z}\left(\frac{1}{s}\right)+\omega_z^2\left(\frac{1}{s}\right)^2}{1+\frac{\omega_p}{q_p}\left(\frac{1}{s}\right)+\omega_p^2\left(\frac{1}{s}\right)^2} \tag{31}$$

This transfer function can now be represented by the state-variable signal-flow graph shown in Fig. 9(a). Using the opamp realization for an integrator, lossy integrator, and summer, we obtain the active opamp version of a general biquad as shown in Fig. 9(b). The transfer function for this circuit is

$$T(s) = \frac{V_{OUT}}{V_{IN}} = \frac{R_2}{R_9}\cdot\frac{s^2+s\left[\frac{\omega_p}{q_p}\left(1-\frac{R_9}{R_{10}}K_b\right)\right]+\left[\omega_p^2\left(\frac{R_9}{R_{11}}K_1-1\right)\right]}{s^2+\frac{\omega_p}{q_p}s+\omega_p^2} \tag{32}$$

where $K_b = R_4/R_1$, $K_1 = R_2/R_1$, $R_7 = R_8$, and

$$K = R_{12}/R_9 \tag{33a}$$

$$\omega_p^2 = \frac{R_8}{R_2R_5R_7C_3C_6} \tag{33b}$$

$$q_p = R_4C_3\omega_p \tag{33c}$$

$$\omega_z^2 = \omega_p^2\left(\frac{R_9}{R_{11}}K_1-1\right) \tag{33d}$$

$$\frac{\omega_z}{q_z} = \frac{\omega_p}{q_p}\left(1-\frac{R_9}{R_{10}}K_b\right) \tag{33e}$$

With this general-purpose biquad, any arbitrary biquadratic filter function can be obtained by selecting the resistors and capacitors to match the desired coefficients, as in Eq. 33(a) to (e). Note, however, that at least three, and in the general case four, opamps are required for its realization. This is the penalty to be paid for the fact that the complex-conjugate pole and zero pairs can be tuned independently of each other. Considering that pole and zero tuning is in itself time-consuming and costly (and, in the case of integrated circuits, only achievable by switching in or out units of capacitor or resistor arrays), it follows that multiple-amplifier biquads are sometimes considered to be impractical from the point of view of both cost and power dissipation. On the other hand, in terms of integrated-circuit (IC) design, in which opamps take up less chip area than capacitors of any practical size, multiple-amplifier biquads are becoming increasingly useful and practical. One reason for this is that pole and zero tuning can be accomplished individually by a single resistor or capacitor (designed especially in arrays of suitably small switchable units) for a pole and zero pair, respectively. Furthermore this biquad has other important advantages as far as IC chip design is concerned. For one thing it uses opamps ex-

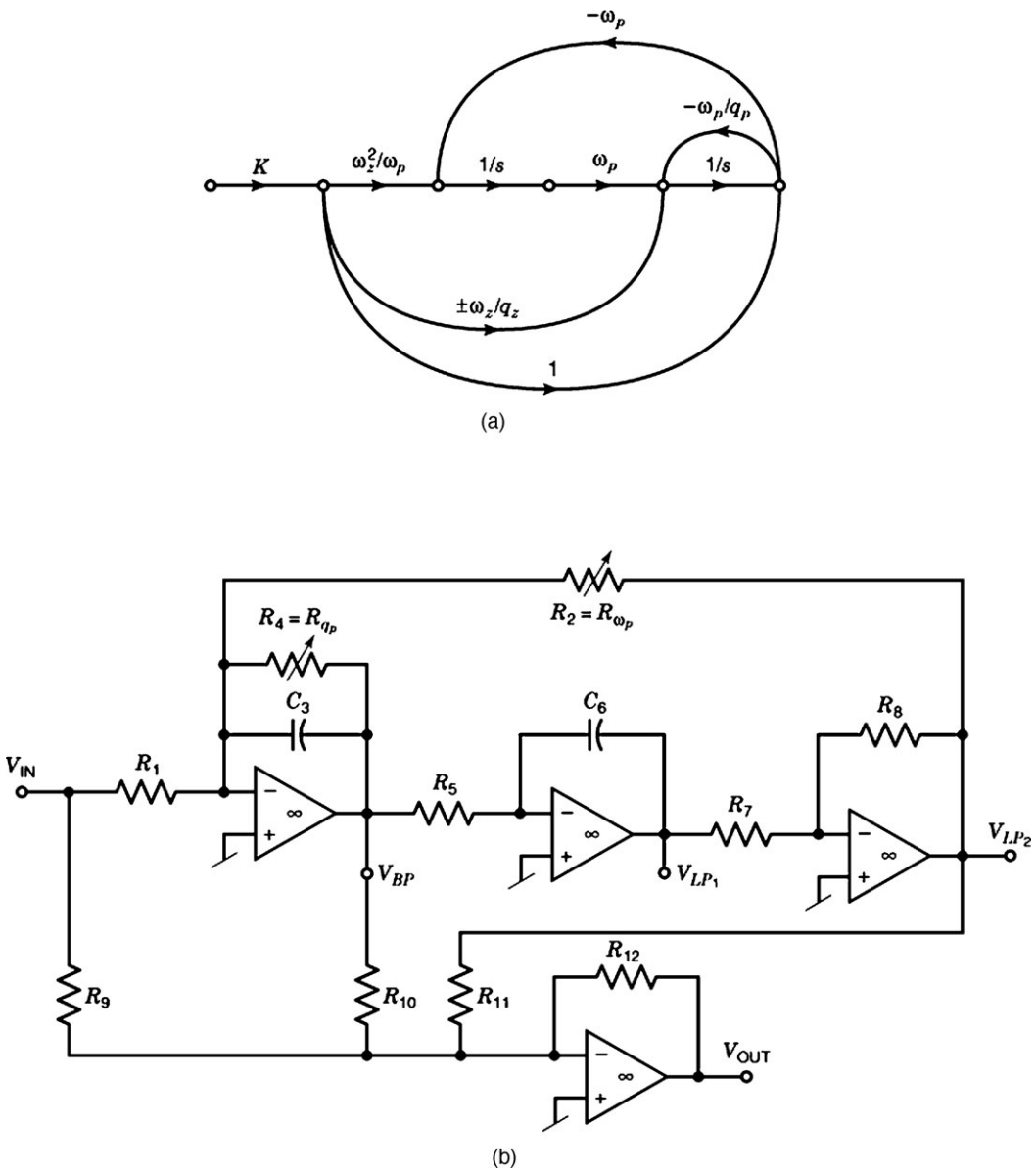

Figure 9. State-variable biquad: (a) signal-flow graph, (b) circuit diagram of the corresponding general-purpose biquad.

clusively in the 'inverting mode', in which the input terminals are at 'virtual ground'. This is a big advantage compared to the single-amplifier biquads, in which opamps are used with input terminals in 'common mode'. The former, compared to the latter, has advantages with respect to 'dynamic range', which becomes increasingly important as the supply voltage is reduced. The trend in IC chip design is to reduce the supply voltage as much as possible in order to reduce power and chip size.

For another, the concept of modular cascades of biquads in filter design provides a flexibility not found in inductorless ladder simulations. In the case of high-selectivity (high-pole-Q) and high-precision applications, the *LC* filter simulation method discussed below, in which inductors are either directly replaced by gyrator–capacitor combinations (*inductor simulation*) or eliminated by the so-called frequency-dependent negative resistor (*FDNR*) transformation, must also be considered. The reason for this is related to the extraordinary sensitivity properties of *LCR* and simulated *LCR* ladder networks. These properties must therefore be discussed first, namely in the following section, before the actual inductor simulation can be dealt with.

SENSITIVITY PROPERTIES OF *LC* LADDER FILTERS

LC ladder filters, terminated at both ends by identical resistors (which are selected according to the desired impedance level of the filter), can be shown to have an extraordinarily low sensitivity to variations of individual component values. Thus, for example, if properly designed and resistively terminated at both ends, the tolerances of the individual components of an *LC* ladder filter may be

permitted to be orders of magnitude larger than the required tolerance of the resulting frequency response in the passband. For example, it may be possible to guarantee a 0.1 dB ripple with components having no more than 1% accuracy, if the order of the *LCR* ladder filter is sufficiently high. This remarkable feature of doubly resistively terminated *LC* ladder filters was first pointed out by H. J. Orchard in 1968, decades after *LC* filters had first come into widespread use. Orchard's theorem, as this low-sensitivity property has come to be called, is the reason why filter designers using other than *LCR* components (e.g., active *RC,* switched-capacitor, digital) attempt to maintain this excellent low-sensitivity property by simulating the behavior and the properties of the equivalent *LC* ladder structure, even though the actual components may be entirely different. Thus, the doubly terminated *LC* ladder structure (real or simulated) plays a central role in filter theory and design, no matter what the technology used for the actual filter realization.

To understand the reason for the low-sensitivity property of LCR ladder filters it is interesting to quote Orchard's own words, namely (2):

> If one designs a flat-passband reactance ladder filter to operate from a resistive source into a resistive load, and arranges that, at the frequencies of minimum loss over the passband, the source delivers its maximum available power into the load, one finds, to a first order of approximation, that, at every frequency in the passband and for every component, the sensitivity of the loss to component tolerances is zero. This is easily checked by noting that, when one has zero loss in a reactance network, a component change, either up or down, can only cause the loss to increase; in the neighbourhood of the correct value, the curve relating loss to any component value must therefore be quadratic, and consequently, $d(\text{loss})/d(\text{component})$ must be zero.

It follows from Orchard's theorem that in any doubly terminated passive *LC* ladder network, the transmission sensitivity in the passband with respect to variations of the components, will *decrease* with *decreasing passband ripple* and with *increasing filter order*. This is counter intuitive and in contrast to most other filter structures (and, indeed, to linear systems), which generally become more prone to instability and to high component sensitivity as the filter complexity and order increase. Moreover, Orchard's theorem explains why, in whatever technology (e.g., active *RC,* digital, switched capacitor), the ladder structure simulating a doubly terminated *LC* ladder network is the preferred structure when high performance is required. Here, performance, pertains to high selectivity and order of the filter, as well as to low tolerance with respect to the passband filter characteristics, and to a low sensitivity to component variations *in the passband*.

Note that Orchard's theorem does not make any claims about insensitivity to component variations in the stop band. Indeed, it can be shown that other structures, such as biquad cascades, may well display a lower sensitivity to component variations in the stop band. However, since the specifications in the passband generally have a higher priority than those in the stop band, Orchard's theorem retains its importance. We should point out, however, that since ladder networks are more difficult to manufacture, be it as *LC* structures or in simulated form, economic considerations nevertheless often dictate the use of biquad cascades or variations thereof. In fact, it will depend on the application and the overall requirements whether biquad cascades or ladder structures (*LC* or simulated) constitute the more appropriate realization. As so often in analog design, the choice of optimum filter circuits will depend on a trade-off between performance characteristics (3). In this case, the trade-off will be between tunability (in favor of biquad cascades) and low sensitivity to component tolerances (in favor of indutorless LC ladder simulation).

ACTIVE INDUCTORLESS LADDER FILTERS

In the preceding section, the remarkable property of low sensitivity to component variations in the passband of *LC* ladder filters is discussed (Orchard's theorem). It is this property that has motivated the simulation of passive *LC* ladder filters by active inductorless ladder filters, in those cases in which real inductors may not be used. This is so in most integrated circuit (*IC*) realizations, since inductors, being three-dimensional devices, are basically incompatible with IC manufacture. In order to understand the principal methods of simulating inductors, we must first discuss some basic network elements that are required for this purpose.

Basic Network Elements

The most important basic network elements necessary for the description and analysis of active *RC* filters are the following:

The Two-Port. The two-port, which represents one of the most elementary concepts of network theory, is shown with a load impedance Z_L in Fig. 10. The two-port can be described by the equations

$$V_1 = AV_2 - BI_2 \tag{34}$$

$$I_1 = CV_2 - DI_2 \tag{35}$$

and

$$Z_L = -\frac{V_2}{I_2} \tag{36}$$

Here, the two-port equations, which fully define the two-port, are given in terms of the elements of the so-called [*ABCD*] or transmission matrix. The corresponding matrix equation is then

$$\begin{bmatrix} V_1 \\ I_1 \end{bmatrix} = \begin{bmatrix} A & B \\ C & D \end{bmatrix} \begin{bmatrix} V_2 \\ -I_2 \end{bmatrix} \tag{37}$$

To obtain the input impedance Z_{IN} in terms of the [*ABCD*] parameters, a simple calculation involving Eqs. (34) to (36)

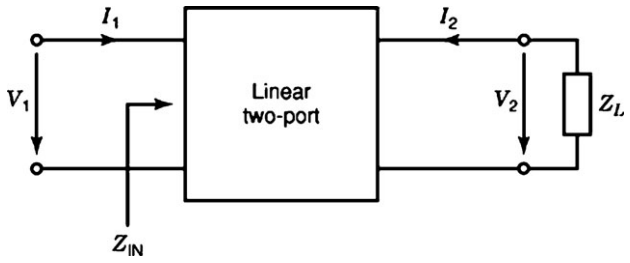

Figure 10. A linear two-port with load Z_L.

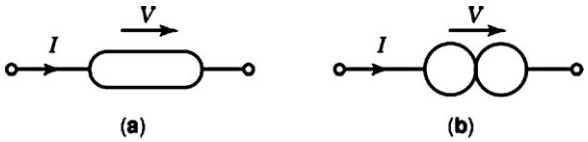

Figure 11. Idealized, physically nonrealizable network elements: (a) nullator; (b) norator.

results in

$$Z_{IN} = \frac{V_1}{I_1} = \frac{AZ_L + B}{CZ_L + D} \tag{38}$$

This expression provides the basis for some of the ideal network elements described further below.

The Nullator, Norator, and Nullor. The nullator and norator belong to a class of physically nonrealizable, idealized network elements that have no conventional matrix representation. Nevertheless, they are very useful in the analysis and synthesis of idealized network elements. Naturally, the idealized network must, at some point, give way to a practical network with physically realizable components. The description of the network with nullators and norators then represents a sort of upper bound, whose idealized performance, due to nonideal effects, can only be approached, but never actually reached.

The nullator [Fig. 11(a)] is defined by the condition

$$I = V = 0 \tag{39}$$

and the norator [Fig. 11(b)] by

$$V = k_1, \qquad I = k_2 \tag{40}$$

where k_1 and k_2 are often said to be "arbitrary." Actually they are not, strictly speaking, arbitrary, but take on values imposed on them by the nullators and the remaining circuitry in which they are embedded. Thus, when a norator is used in a circuit, the voltage V and the current I take on the values needed to satisfy Kirchhoff's current and voltage laws.

An idealized transistor can be represented by a nullator–norator combination as in Fig. 12(a), an idealized operational amplifier (opamp) as in Fig. 12(b). In any given circuit, nullators and norators always occur in pairs, also called *nullors*. The step from an abstract, idealized, and physically nonrealizable nullor circuit to a nonideal, physically realizable circuit is taken by replacing each nullor either by a transistor (transistorization) or by an opamp. Transistorization (in contrast to opamp design) requires

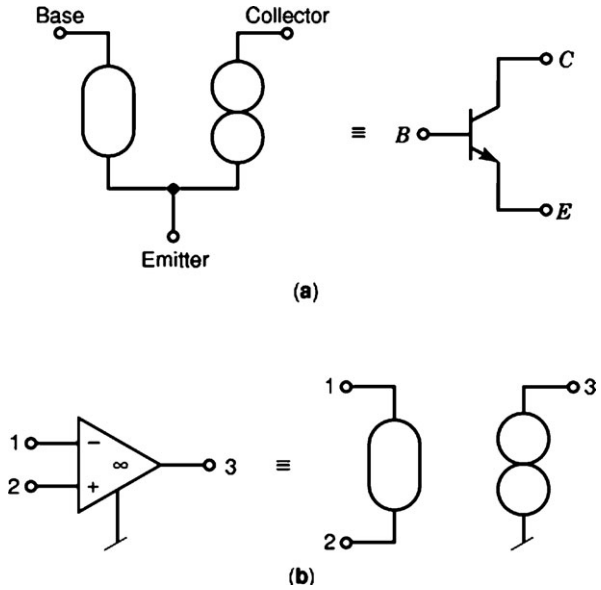

Figure 12. Nullator–norator (nullor) equivalents of two commonly used active devices: (a) transistor, (b) operational amplifier (opamp).

every nullor to have a common terminal, which corresponds to the emitter of the transistor.

The Impedance Converter. The impedance converter is a two-port whose [*ABCD*] matrix is given by

$$[ABCD] = \begin{bmatrix} A & 0 \\ 0 & D \end{bmatrix} \tag{41}$$

If A and D are frequency-dependent [i.e., $A = A(s), D = D(s)$], then we have a *general impedance converter* (*GIC*). For the case that A and D are constants, but of opposite polarity, that is,

$$A = \pm k_1, \qquad D = \pm \frac{1}{k_2} \tag{42}$$

the impedance converter, loaded by Z_L, has, according to Eq. (38), the input impedance

$$Z_{IN} = -k_1 k_2 Z_L \tag{43}$$

We then speak of a negative-impedance converter (*NIC*), because, for $k_1 > 0$ and $k_2 > 0$, and for a realizable (i.e., positive) Z_L, the input impedance of the loaded two-port is negative. Thus, for $k_1 = k_2 = 1$, we have $Z_{IN} = -Z_L$.

A nullor realization of an NIC is shown in Fig. 13. Straightforward application of the defining expressions of the nullator and norator [Eqs. (39) and (40), respectively] gives the input impedance as

$$Z_{IN} = -\frac{Z_1}{Z_2} Z_L \tag{44}$$

Note that in Eq. (42) the pair $A = -k_1$, $D = +k^{-1}{}_2$ corresponds to an NIC with voltage reversal, called a *VNIC*; the pair $A = +k_1, D = -k^{-1}{}_2$ corresponds to an NIC with current reversal, called a *CNIC*. The nullor configuration in

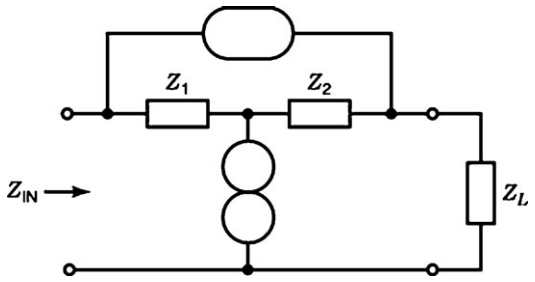

Figure 13. Nullator–norator (nullor) realization of a loaded negative-impedance converter (NIC).

Fig. 13 corresponds to a CNIC; the nullor-dual circuit (i.e., nullator and norator exchanged) results in a VNIC. Note, furthermore, that the configuration in Fig. 13 excludes a one-transistor realization of an NIC because the nullor has no common terminal. Using nullator–norator identities to extend the circuit, a two-transistor realization can be obtained. Such nullator–norator extensions are based on the fact that a nullator and norator in series is equivalent to an open circuit; in parallel such a pair is equivalent to a short circuit.

The Impedance Inverter. An impedance inverter is defined as a two-port whose [*ABCD*] matrix is given by

$$[ABCD] = \begin{bmatrix} 0 & B \\ C & 0 \end{bmatrix} \tag{45}$$

For the special case that

$$B = \frac{1}{g_1}, \qquad C = g_2 \tag{46}$$

the input impedance to the loaded two-port becomes

$$Z_{IN} = \frac{1}{g_1 g_2 Z_L} \tag{47}$$

This is the defining expression for the so-called gyrator, whose symbolic representation is shown in Fig. 14. The gyrator constants $g_1 = g_2$ have the dimensions of inverse resistance, and a capacitively loaded gyrator (see Fig. 14) has an inductive input impedance

$$Z_{IN} = j\omega \frac{C}{g_1 g_2} = j\omega L_{eq} \tag{48}$$

where the equivalent inductance L_{eq} is given by

$$L_{eq} = \left. \frac{C}{g_1 g_2} \right|_{g_1 = g_2 = g} = \frac{C}{g^2} \tag{49}$$

The gyrator–capacitor combination represents the oldest and most common method of simulating an inductance without an actual electromagnetic inductive device being used. The assumption that $g_1 = g_2 = g$ very often holds in practice, although if it does not, inductance simulation still results.

To simulate a floating inductance we require two cascaded gyrators with a grounded capacitor in between them (see Fig. 15). The equivalent inductance is again given by Eq. (48). An *LC* band-stop filter and its gyrator–*R*–*C* simulation are shown in Fig. 16. From Eq. (49) each gyrator constant g_i is given by

$$g_i = \left(\frac{C_{L_i}}{L_i} \right)^{1/2} \tag{50}$$

An impedance inverter consisting of nullors and resistors that has gyrator characteristics is shown in Fig. 17. Typically a gyrator-type impedance inverter requires three nullors for its realization. For the nullor gyrator of Fig. 17 we have

$$[ABCD] = \begin{bmatrix} 0 & R_2 \\ 1/R_1 & 0 \end{bmatrix} \tag{51}$$

Thus, with the load $Z_L = (sC_L)^{-1}$, we have with Eq. (49)

$$L_{eq} = R_1 R_2 C_L \tag{52}$$

Note that the nullators in Fig. 17 are designated n_i, the norators N_i, where $i = 1, 2, 3$; they are all identical, however, and defined by Eq. (39) and Eq. (40), respectively.

The Frequency-Dependent Negative Resistor. The frequency-dependent negative resistor (*FDNR*) is obtained by carrying out a so-called impedance-scaling procedure on an *LCR* network, which is aimed at transforming all the inductors of the *LCR* network into resistors. Impedance scaling implies multiplying all the impedances of a network by a dimensionless constant k, or by a frequency-dependent dimensionless factor $k(s)$. Significantly, when carrying out an impedance-scaling procedure on a network, the transfer function of the network remains unchanged. Thus, letting

$$k(s) = \frac{\omega_0}{s} \tag{53}$$

where ω_0 is arbitrary but often selected equal to the filter cutoff frequency, and scaling each impedance associated with L_i, C_j, and R_v by $k(s)$, the resulting scaled impedances are

$$Z_i' = \omega_0 L_i = R_i' \tag{54a}$$

$$Z_j' = \frac{\omega_0}{s^2 C_j} = \frac{1}{s^2 D_j} \tag{54b}$$

$$Z_v' = \frac{\omega_0}{s} R_v = \frac{1}{sC_v'} \tag{54c}$$

Note that every inductor L_i is transformed into a resistor $R'_i = \omega_0 L_i$, every resistor R_v into a capacitor $C'_v = (\omega_0 R_v)^{-1}$, and every capacitor C_j into a new element $D_j = C_j/\omega_0$. The last is known as a frequency-dependent negative resistor (*FDNR*). The reason for this name is that for $s = j\omega$ (i.e., for a sinusoidal signal) the impedance Z'_j is equal to $-(\omega^2 D_j)^{-1}$, and this negative, frequency-dependent quantity is real and has the dimensions of resistance. The network symbol for the FDNR is shown in Fig. 18(a). The FDNR transformation is most useful for low-pass-type filters comprising numerous floating inductors and grounded capacitors, as

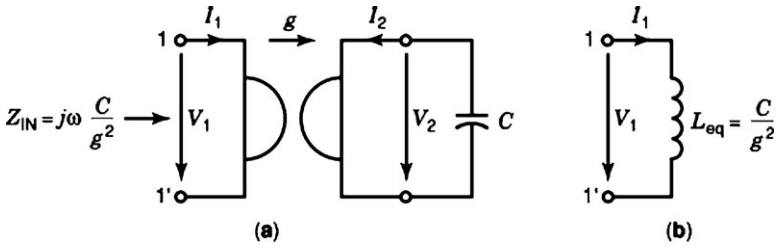

Figure 14. Simulation of a grounded inductor: (a) the gyrator–capacitor combination where $I_1 = -gV_2$, $I_2 = gV_1$; (b) the equivalent inductor given in terms of the capacitor C and the gyrator constant g.

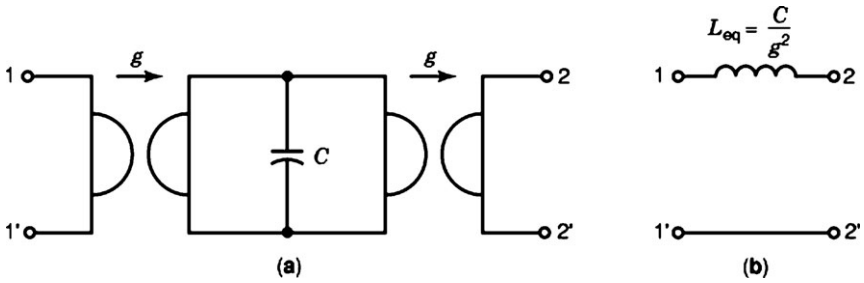

Figure 15. Simulation of a floating inductor: (a) the gyrator–capacitor combination; (b) the equivalent inductor given in terms of the capacitor C and the gyrator constant g.

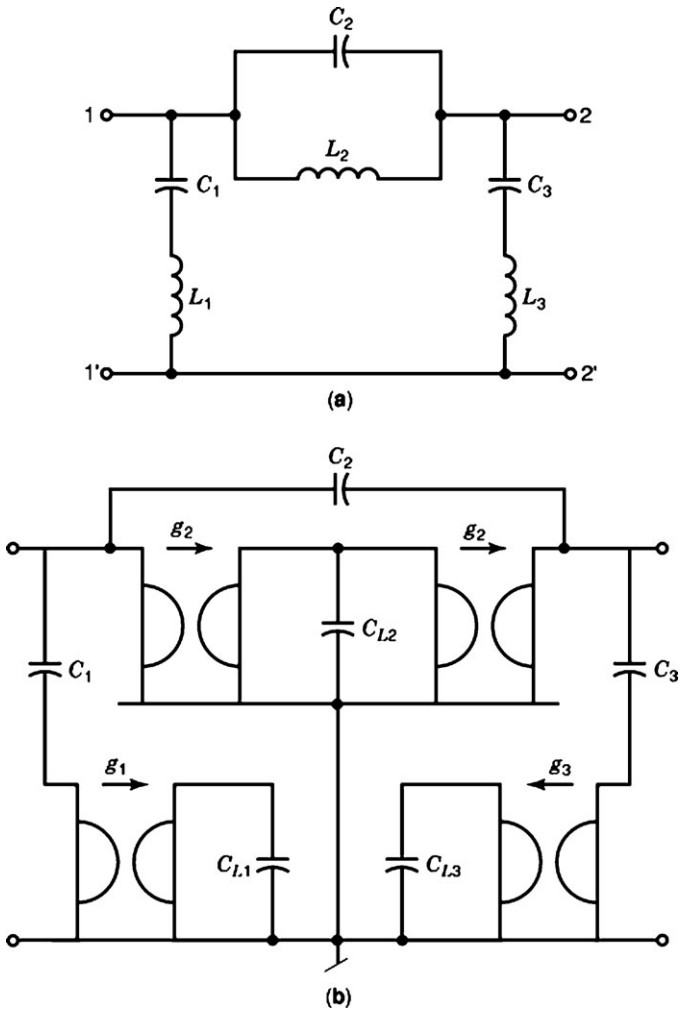

Figure 16. Inductor simulation of an LC band-stop filter: (a) LC band-stop filter; (b) the gyrator–C equivalent filter, where $g_1 = (C_{L1}/L_1)^{1/2}$, $g_2 = (C_{L2}/L_2)^{1/2}$, and $g_3 = (C_{L3}/L_3)^{1/2}$.

shown in the FDNR transformation of a fifth-order elliptic low-pass LCR filter [Fig. 18(b)], into an equivalent inductorless FDNR–RC filter [Fig. 18(c)]. Since in classical filter synthesis every LCR network has a dual network, one of which is a minimum-L and the other a minimum-C network, the FDNR transformation is preferably applied to the minimum-C version so that a maximum number of inductors are transformed into resistors. The fact that the resistive terminations become capacitive may be a problem with the FDNR transformation; the problem can, however,

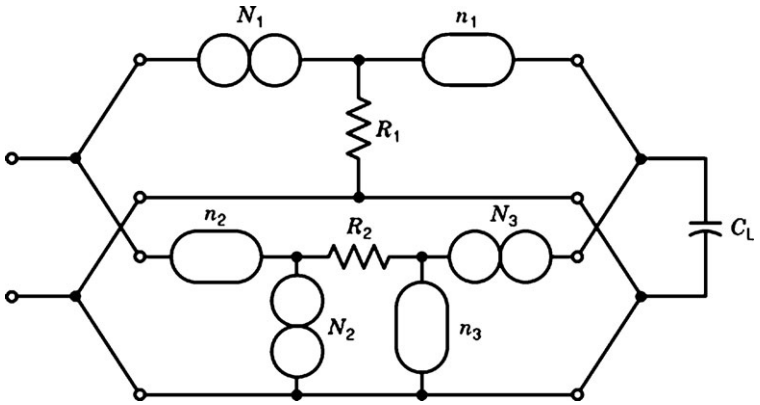

Figure 17. Nullator–norator realization of a gyrator with load capacitor C_L. The gyrator consists of two voltage-controlled current sources (*VCSS*) connected in parallel and in opposite directions. The upper VCS is positive, the lower one is negative.

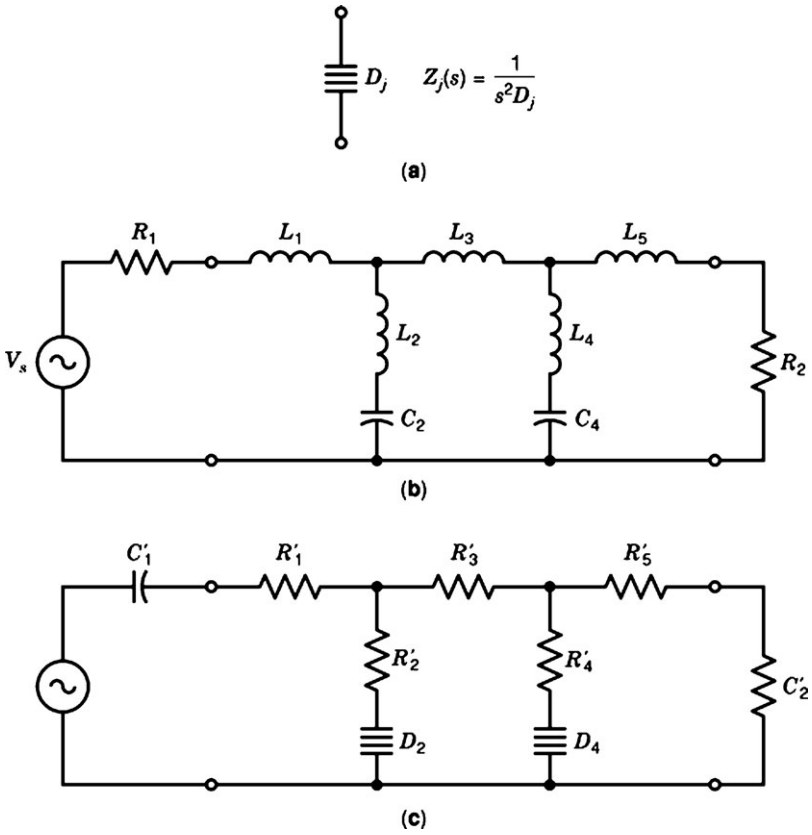

Figure 18. Inductor simulation based on the frequency-dependent negative-resistor (*FDNR*) transformation: (a) FDNR symbol; (b) fifth-order elliptic *LCR* low-pass filter; (c) FDNR-transformed equivalent circuit.

generally be circumvented in a number of ways. One is to connect a large-valued resistor in parallel with the terminating capacitors; another is based on so-called GIC embedding, the principles of which are outlined below under "Active *RC* Simulation of *LCR* Ladder Filters."

The nullor realization of an FDNR can be obtained by cascading two NICs of the kind shown in Fig. 13, resulting in the nullor configuration shown in Fig. 19. It follows from Eq. (44) that the input impedance of this configuration is given by

$$Z_{IN} = \frac{Z_1 Z_3}{Z_2 Z_4} Z_L \qquad (55)$$

Depending on which of the five impedances in this expression are resistive and which capacitive, either an FDNR or a simulated inductor (equivalent to a gyrator–*C* combination) can be obtained. Thus, if any one of the three pairs, (Z_1, Z_3), (Z_1, Z_L), and (Z_3, Z_L), is capacitive and the remaining three impedances are resistive, an FDNR is obtained. Similarly, if either Z_2 or Z_4 is capacitive and the other four impedances resistive, a simulated inductor results.

Using two opamps to replace the two nullors in the configuration of Fig. 19, a working circuit is obtained. Again, there are various ways of combining the nullors (e.g., $[n_1, N_1]$ and $[n_2, N_2]$, or $[n_1\ N_2]$ and $[n_2\ N_1]$), and for each combination, more than one method of connecting the opamps. (Remember, in contrast to a transistor, a nullor being replaced by an opamp requires no common terminal.)

Figure 20 shows an opamp–*RC* realization of the fifth-order FDNR–*RC* low-pass filter of Fig. 18(c). The component selection in terms of resistors and capacitors, combined with the opamp connection to obtain the FDNRs

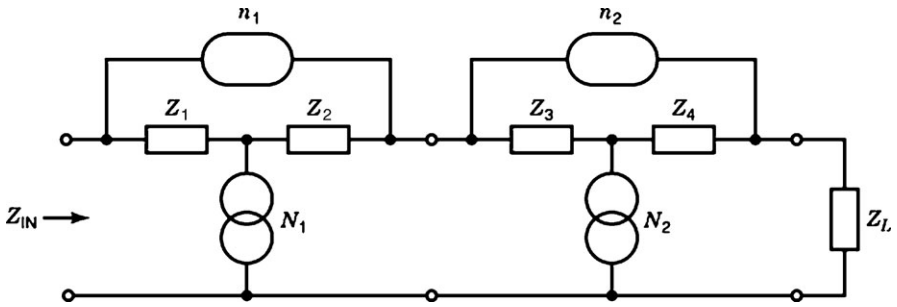

Figure 19. Two nullor-based negative-impedance converters (NICs) in cascade, with loading impedance Z_L. This configuration serves as a basis for gyrator and FDNR design.

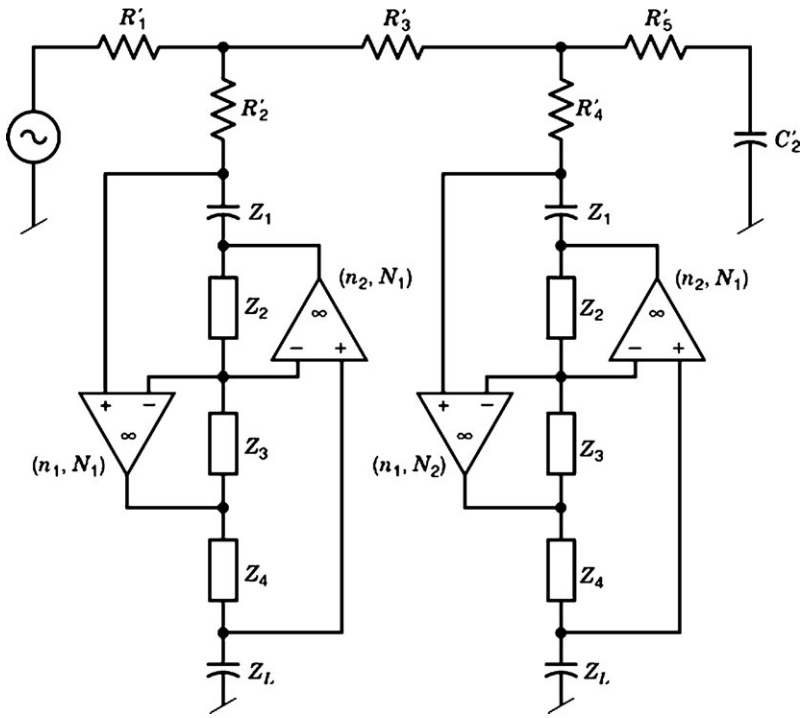

Figure 20. FDNR-based opamp–*RC* realization of the low-pass filter in Fig. 18(c).

shown in Fig. 20, has proved itself well in practice. Notice that in this realisation of the *LCR* filter, the source resistor R_1 in Fig. 18(b) was selected to be zero, in order to guarantee a dc path from source to load. Although this violates Orchard's theorem, which requires equal resistive terminations at the source and load, the penalty involved, in terms of increased component sensitivity, is often acceptable and will generally still be better than it would be with a cascaded-biquad design.

Active *RC* Simulation of *LCR* Ladder Filters

Under "Sensitivity Properties of *LC* Ladder Filters" the remarkable property of low sensitivity to component variations in the passband of *LC* ladder filter structures was discussed (Orchard's theorem). This property has motivated the simulation of *LC* ladder filters in those cases in which high filter performance is required but inductors may not be used, as in integrated-circuit realizations, both analog and digital. It has been shown above that the two most important active elements used to build active-*RC* simulated *LC* ladder filter networks are (1) the gyrator for inductor simulation and (2) the frequency-dependent negative resistor (FDNR), as it occurs in conjunction with the FDNR transformation of *LCR* filter networks. Which of these two approaches is used depends on the *LCR* filter that is to be rendered inductorless. Some illustrative examples will demonstrate this in what follows.

Consider, for example, the fifth-order elliptic low-pass filter shown in Fig. 21. This is the minimum-*L* version of the minimum-*C* filter shown in Fig. 18(b). Simulating the inductors by gyrator–*C* combinations, we obtain the active *RC* simulated inductor circuit shown in Fig. 22. Note that each floating inductor (i.e., L_2 and L_4) requires two gyrators, and each gyrator requires at least two opamps for its realization. This is because, in practice, gyrators are realized by a nullor configuration as shown in Fig. 19, resulting in the two-opamp structures shown in Fig. 20. Thus the gyrator–*C* replacement of L_2 and L_4 will require eight opamps, which for a fifth-order filter is quite uneconomical, with regard to both component cost and dissipated power.

Floating inductors are typical for a low-pass filter, because a true low-pass characteristic must also transmit direct current (*dc*). The floating inductors could, of course, be eliminated by an FDNR transformation. Carrying this transformation out on the *LCR* filter of Fig. 21 would, however, be counterproductive. L_2 and L_4 would indeed be transformed into resistors, but each of the five capacitors

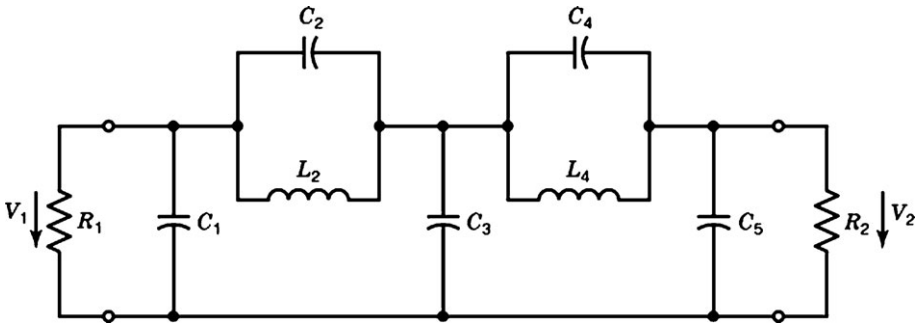

Figure 21. The *LC*-dual, or minimum-*L*, version of the fifth-order elliptic *LCR* low-pass filter of Fig. 18(b).

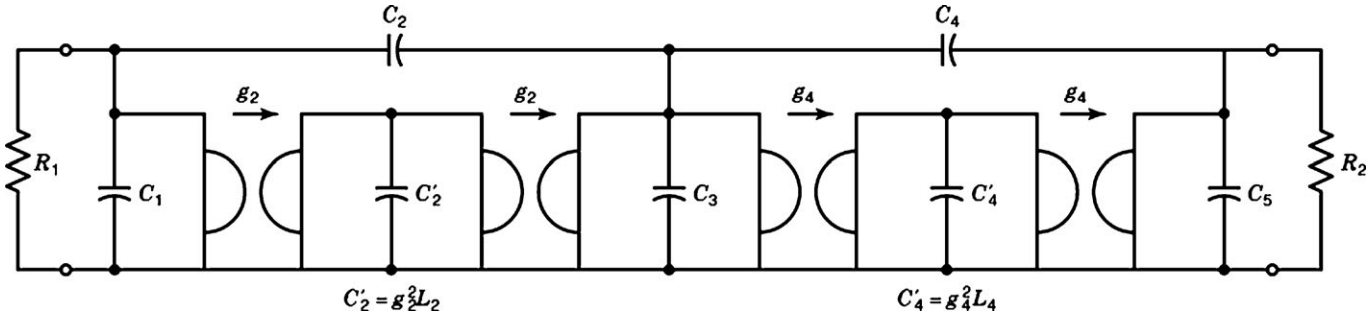

would be transformed into an FDNR. A grounded FDNR can be realized by two opamps; a floating FDNR requires more. Thus, an FDNR transformation of the minimum-*L* filter in Fig. 21 requires well over ten opamps, which is even more extravagant in opamp count than the gyrator–*C* version of Fig. 22.

However, the situation looks quite different for the equivalent minimum-*C* version of a filter. This is the filter shown in Fig. 18(b) and, after impedance scaling by ω_0/s (where ω_0 is selected as the filter cutoff frequency ω_c), corresponds to the FDNR-transformed filter in Fig. 18(c). Here each impedance-scaled inductor L_i becomes a resistor $R'_i = \omega_0 L_i$, each resistor R_j a capacitor $C'_j = (\omega_0 R_j)^{-1}$, and each capacitor C_v an FDNR $Z'_v = (s^2 D_v)^{-1}$, where $D_v = C_v/\omega_0$. Note that there are now only two active elements in the filter: the two impedance-transformed capacitors, each of which becomes a grounded FDNR. With two opamps required for each FDNR, the overall circuit now comprises four opamps, in addition to numerous resistors and capacitors, as shown in Fig. 23. Thus, compared to the simulated inductor version of the filter using gyrators as in Fig. 22, the number of opamps using the FDNR transformation has now been halved.

We now compare the simulated *LC* ladder filter of Fig. 23 with an equivalent cascade of single-ended biquads to realize the same fifth-order low-pass filter. Using typical biquads capable of realizing finite zeros for an elliptic filter, we obtain the circuit configuration shown in Fig. 24. Here the opamp count has been halved again, but this reduction comes at a price. Because the sensitivity to component variations is higher with the biquads than with the simulated *LCR* ladder filter, the performance in the passband of the biquad cascade, when subjected to ambient changes involving temperature, humidity, or aging, will be significantly worse for the biquads than for the simulated *LCR* ladder filter. Furthermore, due to the higher sensitivity

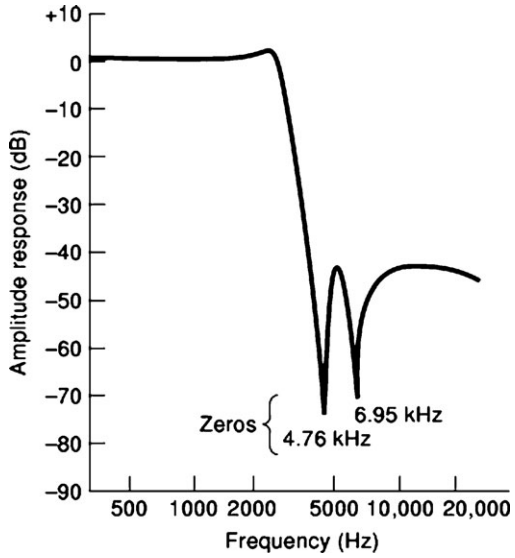

Figure 25. Amplitude response of fifth-order elliptic low-pass filter obtained by measurement of the filter shown in Fig. 23 and in Fig. 24 (nominally, no difference between the two filters can be distinguished).

of the biquads, to obtain an accurate nominal frequency response, either the filter will have to be fine-tuned, or very accurate, low-tolerance, and therefore expensive *RC* components must be used. By contrast, because of its low sensitivity, the FDNR-simulated ladder network of Fig. 23 can be built with less expensive components of reasonable tolerance, while achieving a highly accurate frequency response, often with no fine tuning required. Nominally, however, with ideal components, the filter response of the two filters (shown in Fig. 25) will be identical, and will satisfy the intended specifications.

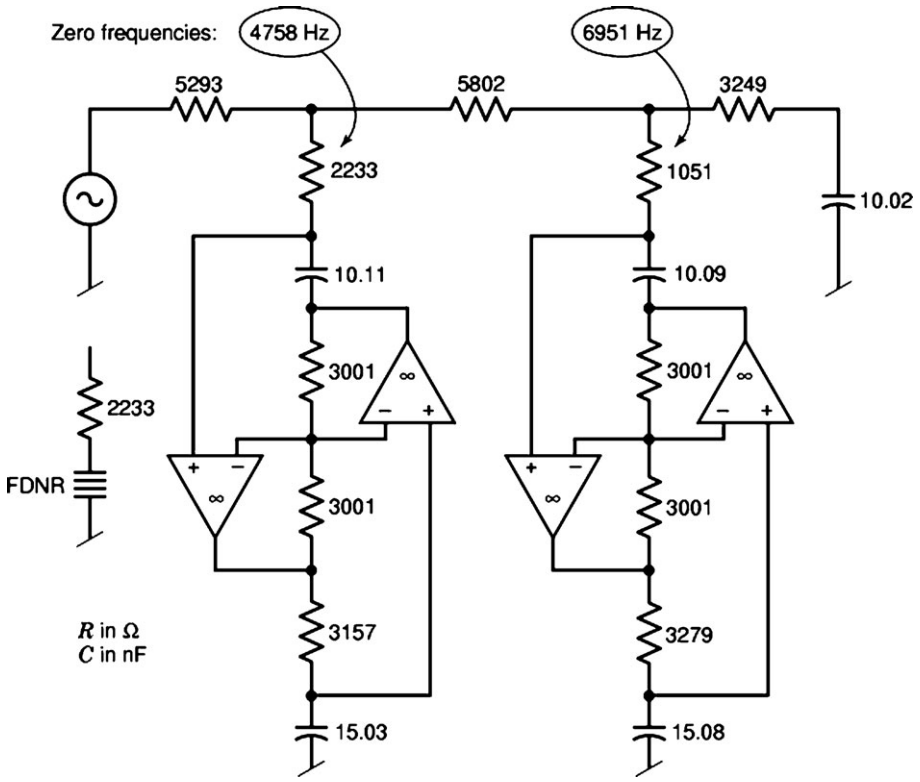

Figure 23. FDNR-based opamp–*RC* realization of the fifth-order elliptic low-pass filter in Fig. 18(c), with component values selected for amplitude response shown in Fig. 25.

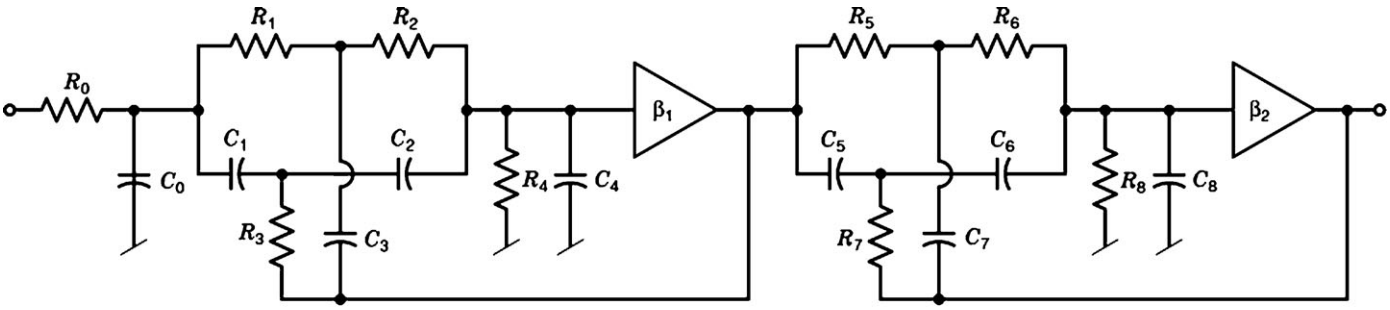

$R_0 = 23068$ $C_0 = 5.6$ $R_1 = 19081$ $R_2 = 19081$ $R_3 = 9540$ $R_4 = 93529$ $C_1 = 1.2$ $C_2 = 1.2$ $C_3 = 2.4$ $C_4 = 2.7$ $\beta_1 = 1.84$ $R_5 = 12389$ $R_6 = 27875$ $R_7 = 8577$ $R_8 = 72462$ $C_5 = 2.7$ $C_6 = 1.2$ $C_7 = 3.9$ $C_8 = 1.5$ $\beta_2 = 1.694$

R in Ω
C in nF

The FDNR transformation generally provides the most efficient (in terms of opamp count) inductorless active *RC* circuit for low-pass specifications, because low-pass filters contain floating coils in order to guarantee a dc path from source to load. Simulated floating inductors require two gyrators per inductor, and, as shown in the preceding example, this may result in twice as many opamps being required as for the corresponding FDNR realization. The FDNR preference will not necessarily hold for any general filter application, however; for general filters a combination of gyrator–*C*, FDNR, and *GIC embedding* will more typically provide the most robust (with respect to component tolerances) and economical inductorless filter. An example to illustrate GIC embedding is shown next.

A general impedance converter, or GIC, was briefly introduced above (under "Basic Network Elements") as a two-port with a transmission, or *ABCD*, matrix given by

$$[ABCD] = \begin{bmatrix} A(s) & 0 \\ 0 & D(s) \end{bmatrix} \tag{56}$$

Loading a GIC with an impedance Z_L at the output terminals, the input impedance results from Eq. (38) as

$$Z_{IN} = \frac{A(s)}{D(s)} Z_L = k(s) \cdot Z_L \tag{57}$$

where $A(s)/D(s)$ is a dimensionless but frequency-dependent quantity designated $k(s)$.

GIC embedding is based on the fact that a two-port, which is characterized by its *ABCD* matrix and *embedded* between two GICs as shown in Fig. 26, has the overall transmission matrix

$$[ABCD]_{Tot} = \begin{bmatrix} 1 & 0 \\ 0 & 1/k_1(s) \end{bmatrix} \begin{bmatrix} A & B \\ C & D \end{bmatrix} \begin{bmatrix} 1 & 0 \\ 0 & 1/k_2(s) \end{bmatrix} = \begin{bmatrix} A & B/k_2(s) \\ C/k_1(s) & D/k_1(s)k_2(s) \end{bmatrix} \tag{58}$$

For $k_1(s) = k(s) = k^{-1}{}_2(s)$ this simplifies to

$$\begin{bmatrix} A & Bk(s) \\ C/k(s) & D \end{bmatrix} \tag{59}$$

Since the dimensionless transfer parameters A and D remain unaltered, and the impedance and admittance parameters are scaled by $k(s)$ and $[k(s)]^{-1}$, respectively, embedding between two GICs is identical with impedance scaling of the embedded network by $k(s)$. If $k(s) = \omega_0/s$, then the embedded network undergoes an FDNR impedance transformation. Thus, for example, a resistive network, embedded between two GICs with $k_1(s) = s/\omega_0$ and $k_2(s) = \omega_0/s$, appears as an all-inductive network, as shown in Fig. 27.

In practice, GIC embedding and gyrator–C substitution of inductors can be applied within the same network, depending on the configuration. This is shown in Fig. 28, where a relatively complex *LCR* band-pass filter is shown in (a) and the equivalent inductorless ladder filter is shown in (b). In the latter, GIC embedding and gyrator–C inductor simulation alternate to provide the most efficient simulated active *RC* ladder filter. Note that the embedding is introduced at the terminal end so as to leave the terminating resistor R (and also the first capacitor C_1) intact. This is the most elegant way of avoiding the R-to-C transformation of the terminal resistors that would otherwise occur in a straightforward FDNR transformation.

OTHER METHODS OF INDUCTORLESS FILTER DESIGN

There are numerous other methods of designing inductorless active RC filters which are developed hand in hand with new emerging IC technologies. Many of these are closely related to CMOS IC technology and use the transconductance gm of CMOS transistors together with CMOS-realized capacitors to provide both the RC time constants and the active gain in current-mode type circuits used for the design of inductorless filters. The basic concepts are very similar to those dealt with above, i.e. they are current-mode versions of the opamp-based voltage-mode circuits described earlier.

Another design technique that has been successfully used for inductorless IC filter chips is that of deriving a signal-flow graph (sfg) equivalent of the original LCR ladder filter satisfying the desired filter specifications. Thus, instead of deriving the sfg from the transfer function as in Fig. 9 above, it is derived from the LCR filter circuit. As in Fig. 9, the sfg is then transformed and manipulated until it consists of branches with only integrators, adders, and inverters. These can readily be realized with CMOS-compatible circuits. In voltage-mode circuits, the integrators consist of opamp-based circuits with a capacitor in the negative feedback path and a resistor connected to the inverting input terminal. A significant advantage of such inverters is that the input terminal is at virtual ground, which, as was pointed out above, is advantageous with regard to maximizing the dynamic range of the filter. Current-mode versions of the sfg integrators also exist, and their use is mainly dictated by the IC technology available.

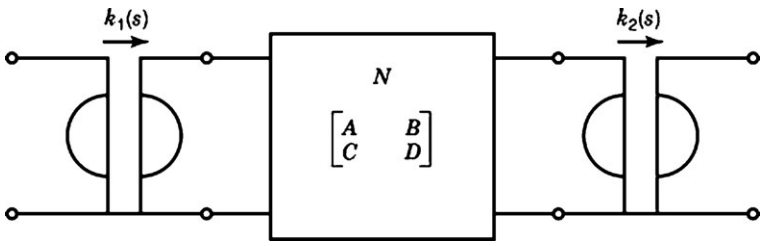

Figure 26. Embedding a network N between two general impedance converters (GICs), with converter constants $k_1(s)$ and $k_2(s)$, respectively.

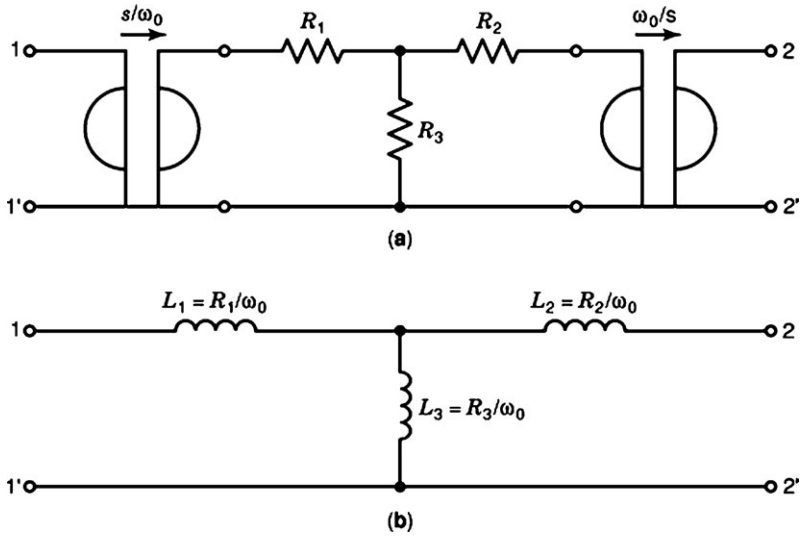

Figure 27. (a) A resistive network embedded between two GICs; (b) the equivalent inductive network.

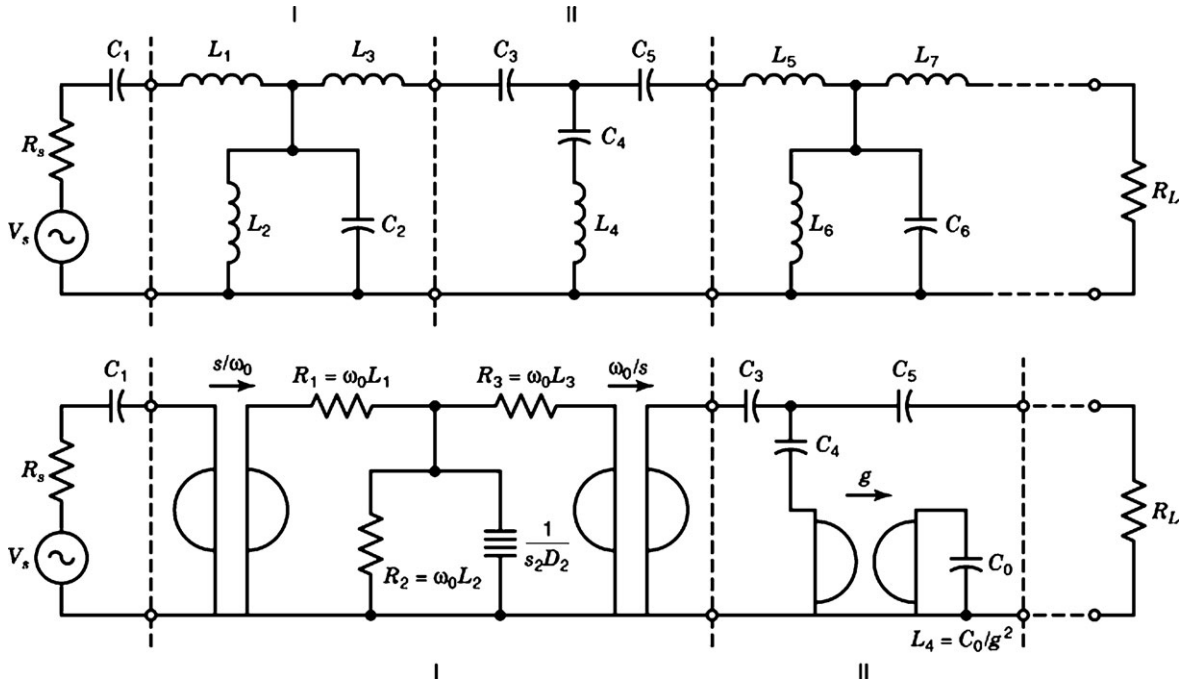

Figure 28. Inductorless simulation of an LC band-pass filter using GIC embedding and gyrator–C substitution of inductors.

BIBLIOGRAPHY

1. R. P. Sallen, E. L. Key, A practical method of designing RC active filters, *IRE Trans. Circuit Theory*, **CT-2**: 78–85, 1955.
2. H. J. Orchard, Inductorless filters, *Electron. Lett.*, **2** (6): 224–225, 1968.
3. C. Toumazou, G. S. Moschytz, and B. Gilbert, *Trade-Offs in Analog Circuit Design*, The Designer's Companion, Kluwer Academic Publishers, 2002.

Reading List

L. T. Bruton, *RC Active Circuits, Theory and Design*, Englewood Cliffs, NJ: Prentice-Hall, 1980.

M. G. Ellis, Sr., *Electronic Filter Analysis and Synthesis*, Norwood, MA: Artech House, 1994.

W. E. Heinlein, W. H. Holmes, *Active Filters for Integrated Circuits*, New York: Springer-Verlag, 1974.

M. Herpy, J. C. Berka, *Active RC Filter Design*, Amsterdam: Elsevier, 1986.

L. P. Huelsman (ed.), *Active RC Filters: Theory and Application*, Stroudsburg, PA: Dowden, Hutchinson and Ross, 1976.

D. E. Johnson, J. L. Hilburn, *Rapid Practical Designs of Active Filters*, Long Beach, CA: Wiley, 1975.

H. Y.-F. Lam, *Analog and Digital Filters: Design and Realization*, Englewood Cliffs, NJ: Prentice-Hall, 1979.

C. S. Lindquist, *Active Network Design with Signal Filtering Applications*, Long Beach, CA: Stewart and Sons, 1977.

S. K. Mitra, *Analysis and Synthesis of Linear Active Networks*, New York: Wiley, 1969.

S. K. Mitra, C. F. Kurth, *Miniaturized and Integrated Filters*, New York: Wiley, 1989.

G. S. Moschytz, *Linear Integrated Networks: Fundamentals*, New York: Van Nostrand Reinhold, 1974.

G. S. Moschytz, *Linear Integrated Networks: Design*, New York: Van Nostrand Reinhold, 1975.

G. S. Moschytz, P. Horn, *Active Filter Design Handbook: For Use with Programmable Pocket Calculators and Minicomputers*, Chichester: Wiley, 1981.

R. Schaumann, M. S. Ghausi, K. R. Laker, *Design of Analog Filters: Passive, Active RC, and Switched Capacitor*, Englewood Cliffs, NJ: Prentice-Hall, 1990.

A. S. Sedra, P. O. Brackett, *Filter Theory and Design: Active and Passive*, Portland, OR: Matrix Publishers, 1978.

M. E. Van Valkenburg, *Analog Filter Design*, New York: Holt, Rinehart and Winston, 1982.

A. B. Williams, *Active Filter Design*, Dedham, MA: Artech House, 1975.

A. B. Williams, F. J. Taylor, *Electronic Filter Design Handbook*, 3rd ed, New York: McGraw-Hill, 1995.

GEORGE S. MOSCHYTZ
Swiss Federal Institute of Technology (ETH), Zürich, Switzerland